Progress In Electromagnetics Research B, Vol. 38, 281–296, 2012

EQUIVALENT CIRCUIT MODEL OF COAXIAL PROBES FOR PATCH ANTENNAS

Y. S. Hu[1], Y.-J. Zhang[2, *], and J. Fan[2]

[1]Department of Mechanical Engineering, Jimei University, 9 Shigu Road, Jimei District, Xiamen, Fujian 361021, P. R. China

[2]EMC Laboratory, Missouri University of Science and Technology, 4000 Enterprise Drive, Rolla, MO 65401, USA

Abstract—An equivalent circuit model of coaxial probes is derived directly from the intrinsic via circuit model. As all the higher-order evanescent modes have been included analytically in the parasitic circuit elements, only the propagating mode needs to be considered by the simplest uniform-current model of a coaxial probe in numerical solvers such as finite element method (FEM) or finite difference time domain (FDTD). This avoid dense meshes or sub-gridding techniques and greatly reduces the computational efforts for accurate calculation of the probe input impedance. The derived equivalent circuit model and the new feeding technique have been validated by both analytical formulas and numerical simulations.

1. INTRODUCTION

Coaxial probes are widely used as feeding structures for microstrip patch antennas as well as other applications. Many authors have found a transverse electromagnetic (TEM) field distribution across the probe aperture is a reasonable approximation for simulations of coaxial probes [1–7]. Therefore, a coaxial probe feeding a patch antenna can be viewed as a mode-converter which converts the TEM mode across the probe aperture into the parallel plate modes. While the higher-order parallel plate modes are usually evanescent waves localized near the probe, the zero-order parallel plate mode can propagate away, excite curtain resonant mode of the entire patch antenna, and thus radiate into surrounding environments. It is much more difficult for numerical

Received 12 December 2011, Accepted 13 January 2012, Scheduled 6 February 2012

* Corresponding author: Yao Jiang Zhang (zhangyao@mst.edu).

methods to obtain accurate input-impedances of a probe than the radiation patterns. It is because input impedance of an antenna is sensitive to the reactive energy stored in the complicated higher-order modes near tiny feeding structures.

Three widely used probe feeding models have been compared in [7] for patch antennas. The simplest one is called uniform-current model which assumes a constant current source along the probe. while it is very easy to implement in numerical methods such as finite element method (FEM) and finite difference time domain (FDTD), the uniform current can only excites the zero-order parallel plate model, i.e., it neglects all the higher-order modes. This means although it can predict the radiation pattern correctly, it cannot get accurate input impedance for a probe-feeding patch antenna with thick substrates [7, 8].

The second model is called magnetic-frill model, in which the TEM field distribution across the probe aperture is assumed and replaced by the equivalent magnetic frill current backed by a perfectly electric conductor wall. It is regarded as the most accurate probe feeding model for both the radiation pattern and the input impedance simulations as all the propagating and evanescent parallel plate modes are included [1–7]. However, magnetic-frill model requires special treatment of the probe exciting source, very dense meshes or sub-gridding (subcell) techniques in FEM and FDTD solvers [9–12]. So the magnetic-frill model usually requires a lot of computing resources and complex mesh-generating technique.

The third feeding technique is gap-feed model, which was well studied in [7]. In this model, the probe is replaced by a conducting rod with one end shorting to one plate and another end having a small gap to another plate. A constant gap voltage source is impressed to excite both zero- and higher-order parallel plate modes. In the gap-feed model, a constant source, instead of the space-varied source in the magnetic-frill model, is used. At the same time, it can also take into account the parasitics caused by the higher-order modes. However, according to the Fourier transform, the amplitude of the modes are determined by the gap size versus the probe height (the separation of two plates). Different gap size leads to different amplitude of each mode and thus different parasitic values. To relate the gap size with the correct parasitic values, an empirical formula is given for the gap size in [7] by comparing the results of the gap-feed model with those obtained by full-wave numerical simulations. Another drawback of the gap-feed model is that in numerical solutions, the small gap structure still requires dense mesh to capture the rapidly varied fields nearby. Therefore, the gap-feed model is still facing similar difficulties in computational resources and mesh generations as the magnetic-frill

model.

This paper provides a novel feeding approach to calculate the probe input impedance, which can achieve the same accuracy as the magnetic-frill model but using the simplest uniform-current model. This is achieved by an equivalent probe circuit derived from the intrinsic via circuit model in which all the higher-order evanescent modes have been considered analytically and only the zero-order propagating mode excited by the uniform-current along the probe needs to be calculated numerically.

In Section 2, the equivalent probe circuit is directly derived from the intrinsic via circuit model derived in [13, 14]. The equivalent probe circuit is a two port network with one coaxial port of the probe and one radial port of the parallel plate waveguide. The radial port impedance reflects the plate geometry and surrounding environments. It provides a new feeding approach as all higher-order evanescent modes have been included analytically. Only the radial port impedance, which reflects the effects of the propagating zero-order mode, needs to be extracted by numerical solvers. Section 3 illustrates how to extract the radial port impedance using the simplest uniform-current model in finite element method (FEM). This means this new approach can achieve the same accuracy of magnetic-frill model yet remain the benefits of uniform-current model in mesh generation as well as computer resources. Section 4 discusses the properties of parasitics and provides several analytical and numerical examples to validate the equivalent probe circuit, which is followed by a short conclusion.

2. RIGOROUS EQUIVALENT CIRCUIT MODEL OF A PROBE

Consider a probe located at the center of a circular patch antenna with radius of R as shown in Fig. 1. Perfect electric/magnetic conductor (PEC/PMC) as well as the non-reflective perfectly matched layer (PML) boundary conditions are used at the outer boundary $\rho = R$. Various boundaries here are beneficial for the validation of the circuit model derived although only PMC boundary is a useful approximation for a patch antenna analysis. The inner and outer radii of the probe are denoted as a and b, respectively. The probe height or the separation of two plates is h. Between two plates is a dielectric material with a relative permittivity of ε_r. Note that a probe in an infinite plate pair, the case studied in [7], is a special case with the PML boundary condition at $\rho = R$.

The input impedance of the probe at the center of a circular plate

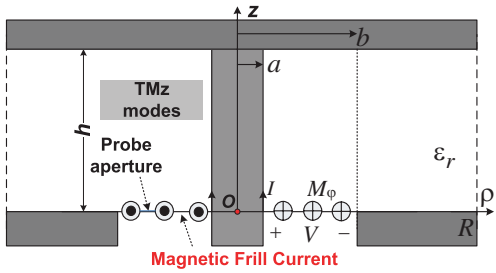

Figure 1. Cross section of a probe in a parallel plate pair.

pair has been derived analytically in (23) of [13] as

$$Y_{\text{in}}^{A} = -\frac{2\omega\varepsilon\pi^2 a}{h\ln(b/a)}\sum_{n=0}^{\infty} F_n^S(a) \tag{1}$$

where

$$F_n^S(\rho) = \frac{(1-\Gamma_a^{(n)}\Gamma_R^{(n)})^{-1}}{k_n(1+\delta_{n0})}\left\{\begin{matrix}\left[H_0^{(2)}(k_nb)-H_0^{(2)}(k_na)\right]+\\ \Gamma_R^{(n)}[J_0(k_nb)-J_0(k_na)]\end{matrix}\right\} \cdot\left[J_1(k_n\rho)+\Gamma_a^{(n)}H_1^{(2)}(k_n\rho)\right] \tag{2}$$

where

$$\Gamma_a^{(n)} = -\frac{J_0(k_na)}{H_0^{(2)}(k_na)} \tag{3}$$

$$\Gamma_R^{(n)} = \begin{cases} -\dfrac{H_0^{(2)}(k_nR)}{J_0(k_nR)} & \rho = R \quad \text{PEC} \\ -\dfrac{H_1^{(2)}(k_nR)}{J_1(k_nR)} & \rho = R \quad \text{PMC} \\ 0 & \rho = R \quad \text{PML} \end{cases} \tag{4}$$

The equivalent circuit of a probe can be derived directly from the intrinsic via circuit model in Fig. 7 of [13] by shorting the coaxial port on the top plate as shown in Fig. 2. It can be seen that the probe can be described as a two-port network with a coaxial port and a radial port. It shows clearly the parasitics due to by the higher-order evanescent parallel plate modes, C_p, as well as those due to the zero-order mode, the capacitance C_0, the inductance L_0 and the transformer ratio R_0. The plate pair can be simply modeled as an impedance of the radial port located at $\rho = b$, the radius of the probe aperture.

We assume any higher-order mode cannot reach the edges of patch antennas. Therefore, C_p is only related to the geometry of

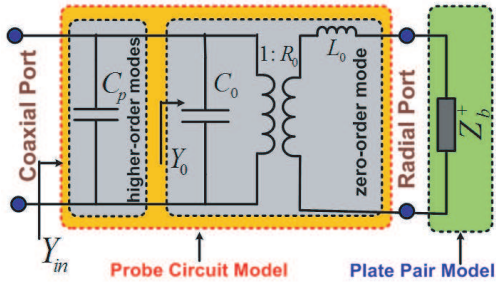

Figure 2. Equivalent probe circuit and its connection with the radial port impedance.

the probe and doesn't vary with the size and shapes of the patch antennas. The admittance Y_0 represents the admittance due to the zero-order or propagating mode. The reason we can use a parasitic capacitance C_p here is that evanescent TM modes or E-modes always store capacitive electromagnetic energy. The capacitance C_p has been given analytically as [13, 15]

$$C_p = \frac{8\pi\varepsilon}{h\ln(b/a)} \sum_{n=1,3,5,\ldots}^{\infty} \frac{\left(1-\Gamma_a^{(n)}\Gamma_R^{(n)}\right)^{-1}}{k_n^2 H_0^{(2)}(k_n a)} \cdot \left\{ \begin{array}{l} \left[H_0^{(2)}(k_n b) - H_0^{(2)}(k_n a)\right] + \\ \Gamma_R^{(n)}\left[J_0(k_n b) - J_0(k_n a)\right] \end{array} \right\}. \tag{5}$$

Here, we assume that all the higher-order parallel plate modes decay so rapidly away from the probe that they cannot reach to the plate-pair edges. This means for C_p calculation, the reflection coefficients $\Gamma_R^{(n)}$ can be put to be zero for any $n \geq 1$. In other words, for any higher-order mode, the parallel plate seems infinite large. Then, (5) can be simplified as

$$C_p = \frac{8\pi\varepsilon}{h\ln(b/a)} \sum_{n=1,3,5,\ldots}^{N} \frac{\left[H_0^{(2)}(k_n b) - H_0^{(2)}(k_n a)\right]}{k_n^2 H_0^{(2)}(k_n a)} \tag{6}$$

Using the identity $H_0(-jx) = j\pi/2K_0(x)$, it can be further written as

$$C_p = \frac{8\pi\varepsilon}{h\ln(b/a)} \sum_{n=1,3,5,\ldots}^{N} \frac{1}{\nu_n^2}\left[1 - \frac{K_0(\nu_n b)}{K_0(\nu_n a)}\right] \tag{7}$$

where $K_0(\cdot)$ is the zero-order modified Bessel function of the second kind and $\nu_n = jk_n = \sqrt{(n\pi/h)^2 - k_0^2\varepsilon_r}$. Note that the number N is

used to denote the truncated mode number in the practical summation of (6) and (7).

The capacitance C_0, the inductance L_0 and the transformer ratio R_0 can be expressed in their concise forms as [13]

$$L_0 = -\frac{\mu h}{2\pi kb}\frac{W_{00}(kb,ka)}{W_{10}(kb,ka)} \tag{8}$$

$$C_0 = \frac{j\varepsilon\pi^2 a}{kh\ln(b/a)}\frac{W_{10}(ka,ka)}{W_{10}(kb,ka)} \times [W_{10}(kb,kb) - W_{10}(kb,ka)] \tag{9}$$

$$R_v = \sqrt{-R_m R_e} \tag{10}$$

where

$$R_m = \frac{j\pi}{2\ln(b/a)}\frac{W_{10}(kb,kb)}{W_{10}(kb,ka)} \times [W_{00}(kb,ka) - W_{00}(ka,ka)] \tag{11}$$

$$R_e = \frac{a}{b}\frac{W_{10}(ka,ka)}{W_{10}(kb,ka)} \tag{12}$$

where an auxiliary function $W_{mn}\,(x,\,y)$ defined as a determinant of the Bessel and Hankel functions

$$W_{mn}(x,y) = \begin{vmatrix} J_m(x) & J_n(y) \\ H_m^{(2)}(x) & H_n^{(2)}(y) \end{vmatrix}. \tag{13}$$

Thus we have derived a formula to calculate the input admittance of a probe in a circular plate pair as

$$Y_{\text{in}} = j\omega(C_p + C_0) + \frac{R_0^2}{j\omega L_0 + Z_b^+} \tag{14}$$

where Z_b^+ is the outward impedance of the radial port at $\rho = b$. For the probe at the center of a circular plate pair given in Fig. 1, analytical Z_b^+ is

$$Z_b^+ = \frac{j\omega\mu h}{2\pi kb}\frac{H_0^{(2)}(kb) + \Gamma_R^{(0)} J_0(kb)}{H_1^{(2)}(kb) + \Gamma_R^{(0)} J_1(kb)} \tag{15}$$

where $J_{0(1)}(\cdot)$ and $H_{0(1)}^{(2)}(\cdot)$ denote the zero- (first-) order Bessel function and the zero- (first-) order Hankel functions of second kind, respectively.

For a probe in an irregular plate pair, the radial waveguide impedance Z_b^+ cannot be obtained analytically for an irregular plate pair, as in (15) for a circular plate pair. Next section will use FEM as an example to explain how to extract the impedance Z_b^+ for any irregular plate pair using the uniform-current model.

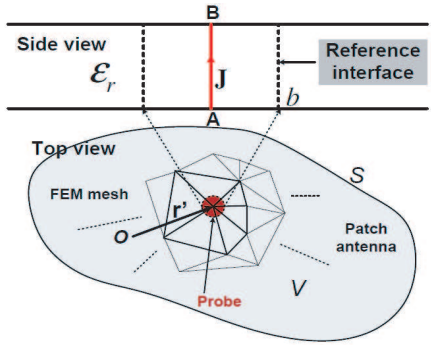

Figure 3. Finite element method extraction of the input impedance of a probe in an irregular patch antenna.

3. PLATE PAIR IMPEDANCE BY NUMERICAL METHODS

For example, consider a probe excite a patch antenna as shown in Fig. 3. The electric field inside the region V can be formulated into an equivalent variational problem with a functional given by [16, 17]

$$F(\mathbf{E}) = \frac{1}{2}\int_V \left(\nabla\times\mathbf{E}\cdot\nabla\times\mathbf{E} - k_0^2\varepsilon_r\mathbf{E}\cdot\mathbf{E}\right)dV + jk_0\eta\left[\int_V \mathbf{E}\cdot\mathbf{J}dV + \int_S \mathbf{E}\times\mathbf{H}\cdot\mathbf{n}dS\right] \quad (16)$$

where $\mathbf{J}$ is the assumed probe current located at $\mathbf{r} = \mathbf{r}'$ from the point A on the bottom plate to the point B on the top plate, and $\mathbf{H}$ is the magnetic field. $\mathbf{n}$ is the unit normal vector of the boundary S.

In the uniform-current model, the probe current is supposed to be constant along the probe as

$$\mathbf{J}(\mathbf{r}) = \delta(\mathbf{r}-\mathbf{r}')\mathbf{e}_{AB} \quad (17)$$

where $\mathbf{e}_{AB}$ is the unit vector along the probe. Following the routine FEM procedure, the electric fields on each node or edge can be obtained [16, 17]. Then, the input impedance can be calculated by an integration along the probe as

$$Z_{\text{in}}^U = \int_A^B \mathbf{E}\cdot\mathbf{e}_{AB}dl \quad (18)$$

Note that the infinitesimal current filament $\mathbf{J}(\mathbf{r})$ is an approximation for the current along the probe surface of $\rho = a$. Therefore, the impedance Z_{in}^U can be regarded as the outward radial impedance at $\rho = a$ of the radial waveguide defined at the center of

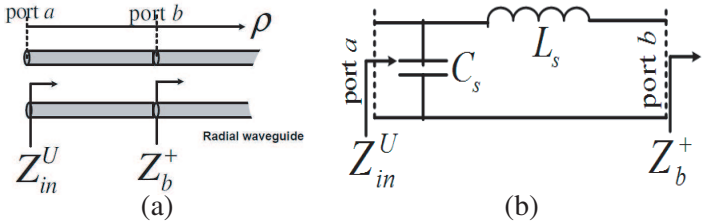

Figure 4. (a) A segment of radial waveguide, (b) the approximate circuit for the small segment of radial waveguide.

the probe instead of that at $\rho = b$ of Z_b^+ which is required in the probe circuit model of Fig. 2. Therefore, we need to derive radial impedance transform between the radial port at $\rho = a$ and that at $\rho = b$. Here, a simple LC is used to connect these two radial ports because it is a very electrically small segment of a radial transmission line as shown in Fig. 4.

The input impedance at port a can be expressed from (15) as

$$Z_a^+ = \frac{j\omega\mu h}{2\pi ka} \frac{H_0^{(2)}(ka) + \Gamma_b J_0(ka)}{H_1^{(2)}(ka) + \Gamma_b J_1(ka)} \tag{19}$$

where Γ_b is the reflection coefficient of the zero-order radial waveguide mode at port b. As the probe is usually electric small comparing to the operating frequency, this segment of the radial waveguide can be approximately represented by a LC-circuit as shown in Fig. 4(b). Using PEC and PMC boundary conditions at $\rho = b$ respectively, inductance L_s and C_s can be derived from (19) as

$$L_s = \frac{Z_a^+}{j\omega} = \frac{\mu h}{2\pi ka} \frac{W_{00}(kb, ka)}{W_{01}(kb, ka)} \tag{20}$$

$$C_s = \frac{1}{j\omega Z_a^+} = \frac{-2\pi a\varepsilon_0\varepsilon_r}{kh} \frac{W_{11}(kb, ka)}{W_{10}(kb, ka)} \tag{21}$$

Note that in the derivation of L_s, the capacitance C_s is neglected. Assuming ka and kb are very small in the frequency of interests, L_s and C_s can be simplified using the small argument approximation of Bessel/Hankel functions as

$$L_s \simeq L_s' = \frac{\mu h}{2\pi} \ln \frac{b}{a} \tag{22}$$

$$C_s \simeq C_s' = \frac{\pi \left(b^2 - a^2\right) \varepsilon_0\varepsilon_r}{h} \tag{23}$$

Clearly, C_s is the parallel plate capacitance of the concentric plate pair ring with inner and outer radii of a and b, and L_s is a radial loop

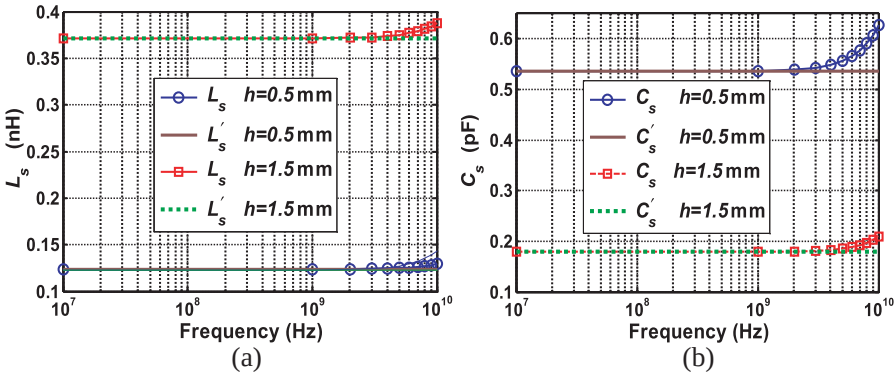

Figure 5. A probe with inner and outer radii of 0.635 mm and 2.188 mm in a dielectric material of relative permittivity of 2.2. (a) L_s and L_s'. (b) C_s and C_s'.

inductance from the port at $\rho = a$ to the port at $\rho = b$. Fig. 5 shows that the frequency-dependent L_s and C_s can be simplified by as the constant L_s' and C_s' at low frequencies.

From the equivalent circuit shown in Fig. 4(b), the impedance Z_b^+ can be extracted from Z_{in}^U by

$$Z_b^+ = \frac{Z_{\text{in}}^U}{1 - j\omega C_s Z_{\text{in}}^U} - j\omega L_s \tag{24}$$

Therefore, the input admittance or impedance of the probe in an irregular patch antenna can be accurately extracted by substituting (24) into (14) as

$$Y_{\text{in}}^C = j\omega(C_p + C_0) + \frac{R_0^2}{j\omega(L_0 - L_s) + \frac{Z_{\text{in}}^U}{1 - j\omega C_s Z_{\text{in}}^U}}. \tag{25}$$

Comparing (22) with (60) in [13], it is clear that we have $L_s = L_0$. Therefore, (25) can be simplified as

$$Y_{\text{in}}^C = j\omega(C_p + C_0) + R_0^2\left(1 - j\omega C_s Z_{\text{in}}^U\right) Y_{\text{in}}^U \tag{26}$$

(26) can be regarded as an improved input admittance of patch antenna from the input admittance by unform constant current model, Y_{in}^U, and the parasitics caused by the higher-order evanescent modes. At low frequencies, we have $R_0 \simeq 1$ and $j\omega C_s \leq 1$, then

$$Y_{\text{in}}^C = j\omega(C_p + C_0) + Y_{\text{in}}^U \tag{27}$$

Clearly, the equivalent probe circuit can improve the accuracy of the input impedance calculation by the unform current model by

considering the higher-order modes with the parasitic capacitance C_p and C_0.

Clearly, C_p, the capacitance from the probe barrel to the unconnected plate due to the higher-order modes is the critical parameter in the input impedance calculation. For a probe in a thin substrate, C_p is too small to affect the first resonant frequency of the patch antenna. However, C_p increases with the thickness of the substrate and becomes unable to be neglected as demonstrated in [8, 19].

The admittance (or impedance) obtained by FEM or FDTD using the uniform-current model can be regarded as an approximation of Y_{in}^U which is defined at the port a at $\rho = a$. (26) is a good approximation for the input impedance evaluation and will be validated by both analytical formulas and numerical examples in next section.

4. VALIDATIONS AND DISCUSSIONS

4.1. Properties of the Parasitics

Using the above derived formulas, Fig. 6 investigates the properties of the parasitics versus frequencies. It can be seen that at lower frequencies (less than 20 GHz for this case), all the parasitics almost remain as constant values for a typical probe. This verifies the derived lumped parasitics in the probe circuit model. Note that from Fig. 6(a), the transformer ratio R_0 is almost not varied with the probe height or plate separation h. At lower frequency, R_0 is almost one but increases rapidly with frequencies after 10 GHz. It can even reach nearly 3 at 40 GHz, which is not negligible.

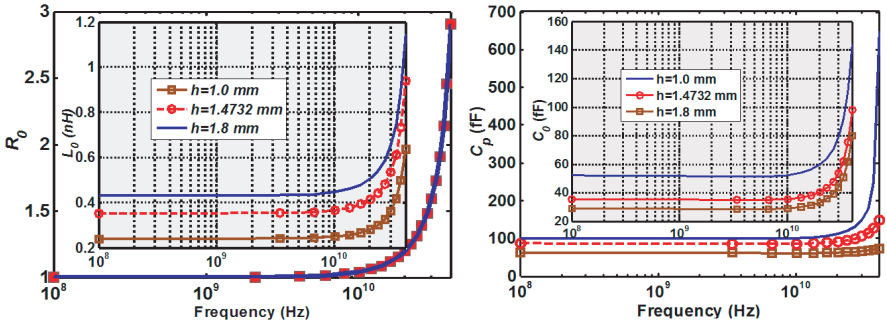

Figure 6. Frequency dependence of the parasitics R_0, L_0, C_p and C_0 ($a = 0.254\,\text{mm}$, $b = 0.8384\,\text{mm}$, $\varepsilon_s = 4.3$, $\varepsilon_\infty = 4.1$, $\tau = 3.1831 \times 10^{-11}\,\text{s}$).

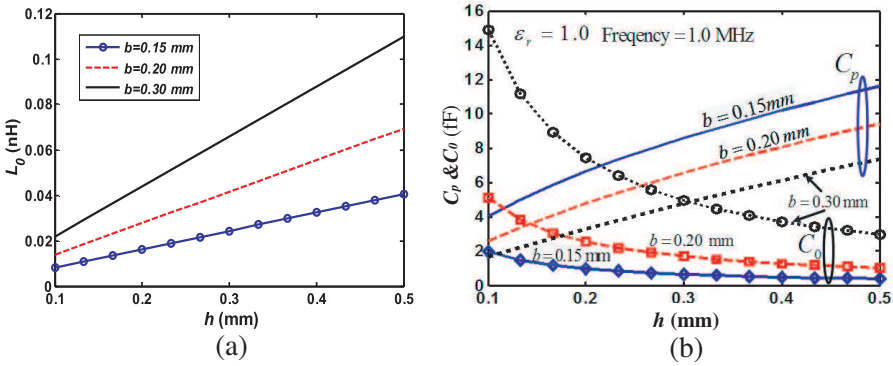

Figure 7. Parasitics L_0, C_p and C_0 versus the separation h of the plate pair ($a = 0.1$ mm, $\varepsilon_r = 1.0$, frequency is 1 MHz).

Figure 7 provides the variations of the parasitics with different outer radius of the coaxial probe and probe height. It shows in Fig. 7(a) that the inductance L_0 increase linearly with the increase of probe heights. Also the larger outer radius leads to large probe inductance. This agrees with the fact that the probe inductance L_0 is the input impedance of a small segment of a radial waveguide terminated by a short circuit. Fig. 7 indicates that with the increase of the probe aperture radius b, C_p decreases but C_0 increases. Moreover, larger probe height results larger C_p but smaller C_0.

4.2. Probe in a Circular Patch Antenna

To validate the probe equivalent circuit derived above, a probe in a circular plate pair is studied whose analytical input impedance has been given in (1). The radii of the probe inner and outer conductor are 0.254 mm and 0.8384 mm, respectively. The separation of the top and bottom plate is 1.4732 mm. The embedded dielectric is described as one term Debye model whose parameters are, respectively, 4.1 for relative infinity permittivity, 4.3 for static permittivity and 3.1831×10^{-11} seconds for its relaxation time.

Figure 8 compares both the real and imaginary parts of the probe in an infinite plate pair using (1) and (14) while the reflection coefficient $\Gamma_R^{(n)}$ vanishes in the calculations. It can be seen that the analytical formula of Z_{in}^A obtained in (1) agrees very well with that obtained by the probe equivalent circuit in (14). The maximum relative error is 2.5%. Fig. 9 compares the input impedance of the plate pair with a radius of 200 mm with PML and PMC boundaries. It clearly shows that the discretized resonant frequencies of the finite cavity of the patch

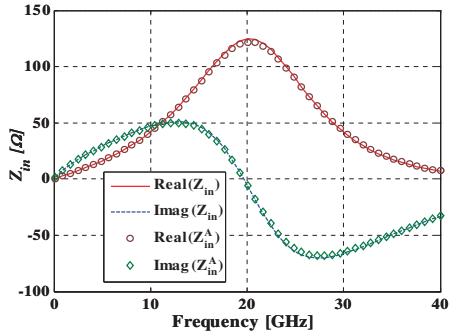

Figure 8. Comparison of the real and imaginary parts of the probe input impedance in an infinite plate pair obtained by the equivalent circuit and the analytical formula.

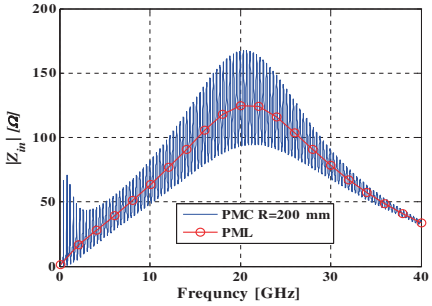

Figure 9. The input impedance of a probe in a circular plate pair with PMC and non-reflective PML boundaries ($R = 200\,\text{mm}$).

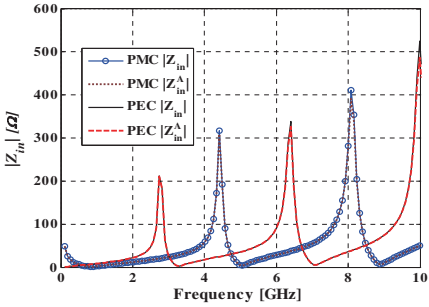

Figure 10. Comparison of the input impedance of a probe in a circular plate pair with PMC and PEC boundaries at $\rho = 20\,\text{mm}$ by analytical formula of (1) and the equivalent probe circuit of (14).

antenna is strongly correlated to the the continuous resonant spectrum of the infinite 'cavity' of the patch, especially at high frequencies.

For a circular patch with a radius of 20 mm with PMC and PEC edge boundary conditions, Fig. 10 compares the input impedance using (1) and (14). Again, excellent agreement between two formulas is observed.

Both Figs. 8 and 10 indicate that the derivation of the equivalent probe circuit is correct no matter what kinds of edge boundary conditions. This also proves that the parasitics in the probe circuit are really intrinsic parameters which are valid for any irregular patch antennas.

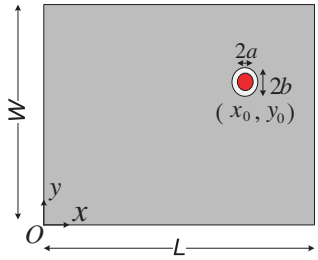

Figure 11. A coaxial probe feeding for a rectangular patch antenna.

4.3. Probe in a Rectangular Patch Antenna

A rectangular microstrip patch antenna is, as shown in Fig. 11, used to validate the derived equivalent circuit feeding model for a coaxial probe. The length, width and height of the patch are L, W and h respectively. The relative permittivity of the substrate is denoted as ε_r. The probe is located at (x_0, y_0) and its inner and outer conductor radii are a and b, respectively.

A rectangular patch, as an example for an irregular patch antenna, is chosen due to the reason that an analytical port impedance, called cavity model, available as given in [18] or (18) in [7], can be regarded as an approximation to the impedance Z_{in}^U in the probe circuit model in case of electrically small probes. Furthermore, the patch antenna can be analyzed by a two dimensional (2D) FEM for extraction of Z_{in}^U using the uniform-current model. Then, the probe circuit derived in this paper can be used to obtain more accurate probe input impedance using (25) as it includes the capacitance, C_p, due to the higher-order modes.

Figure 12 shows the input impedance of a probe in a square patch antenna with different substrate thickness. The sidewall length of the patch is 28.3 mm and the substrate is a material with a relative permittivity of 2.33 and a loss tangent of 0.02. A probe is located at (15.565, 20.565) mm and with inner and outer radii of $a = 0.635$ mm and $b = 2.1884$ mm.

The first resonant frequency of the cavity is 3.4724 GHz (TM_{10} mode). However, the resonant frequency shifts to 3.41 GHz in the case of a thick substrate of 5 mm. The main reason is that the capacitance C_p increases from 34.47 fF when $h = 1$ mm to 146.25 fF when $h = 5$ mm.

It can be seen that for a thin substrate of 1 mm, 2D FEM corrected by the probe circuit given in (25) agrees very well with the cavity model in either the input amplitude or the resonant frequency of the

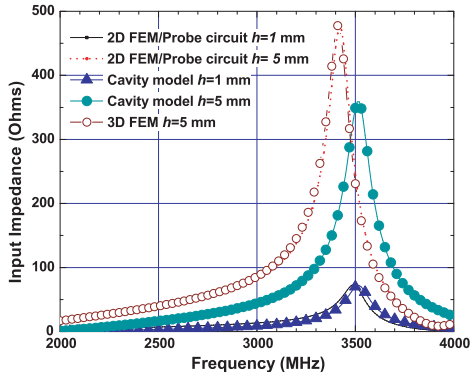

Figure 12. Comparison of input impedance obtained by the probe circuit model, 2D FEM and 3D FEM for a probe in a rectangular patch antennas ($W = L = 28.3\,\text{mm}$, $(x_0, y_0) = (15.565, 20.565)\,\text{mm}$, $a = 0.635\,\text{mm}$ and $b = 2.1884\,\text{mm}$; $\varepsilon_r = 2.33$, $\tan\delta = 0.02$).

patch antenna. For the thick substrate of 5 mm, however, the cavity model cannot match the 3D FEM results obtain by HFSS (Ansoft, Inc.) because it neglects all higher-order modes excited by the probe.

On the other hand, 2D FEM with probe circuit by (25) can predict the resonant frequency shift due to the parasitics caused by the think substrate and agree very well with the results by 3D FEM of HFSS. Therefore, the equivalent probe circuit model is validated.

5. CONCLUSIONS

An equivalent probe circuit is first derived rigorously through electromagnetic analysis for a probe located at the center of a circular patch antenna, and then the probe circuit is proved to be intrinsic and valid for any irregular patch antennas. As all parasitics caused by the evanescent higher-order modes have been evaluated analytically, only the radial impedance due to the propagating zero-order mode requires numerically calculation. Therefore, the simplest uniform-current model can be used to extract the radial impedance in numerical solvers, such as finite element method. This avoids computational burdens caused by dense meshes or sub-gridding techniques for modeling the complicated higher-order modes near the probe. Analytical and numerical examples are provided to validate the probe circuit derived. The new method is as simple as the uniform-current model, and at the same time, it is as accurate as the magnetic-frill model for probes in any irregular patch antennas.

ACKNOWLEDGMENT

Great thanks to the support of science and technology plan project (JA11162) provided by Fujian Provincial Department of Education.

REFERENCES

1. Zheng, J.-X. and D. C. Chang, "End-correction network of a coaxial probe for microstrip patch antennas," *IEEE Trans. on Antenna and Propagat.*, Vol. 39, No. 1, 115–118, Jan. 1991.
2. Vandenbosch, G. A. E. and A. R. Van de Gapelle, "Admittance of coaxial feed between two finite parallel conductors," *Electronics Letters*, Vol. 28, No. 19, 1780–1781, 1992.
3. Wu, B. and H. L. Lo, "Methods and designs for improving the signal integrity of vertical interconnects in high performance packaging," *Progress In Electromagnetics Research*, Vol. 123, 1–11, 2012.
4. Lamultree, S. L. and C. Phongcharoenpanich, "Full-wave investigations of a probe-excited rectangular ring antenna by method of moments with rwg basis functions," *Progress In Electromagnetics Research C*, Vol. 8, 161–177, 2009.
5. Cho, Y. H., "Analytic and numerically efficient scattering equations for an infinitely flanged coaxial line," *Progress In Electromagnetics Research Letters*, Vol. 28, 149–158, 2012.
6. Huang, W.-T., C.-H. Lu, and D.-B. Lin, "Suppression of crosstalk using serpentine guard trace vias," *Progress In Electromagnetics Research*, Vol. 109, 37–61, 2010.
7. Xu, H., D. R. Jackson, and J. T. Williams, "Comparison of models for the probe inductance for a parallel plate waveguide and a equivalent circuit model of coaxial probes for patch antennas 19 microstrip patch," *IEEE Trans. on Antennas and Propagat.*, Vol. 53, No. 10, 3229–3235, Oct. 2005.
8. Davidovitz, M. and Y. T. Lo, "Input impedance of a probe-fed circular microstrip antenna with thick substrate," *IEEE Trans. on Antennas and Propagat.*, Vol. 34, No. 7, 905–911, Jul. 1986.
9. Gong, J. and J. L. Volakis, "An efficient and accurate model of the coax cable feeding structure for FEM simulation," *IEEE Trans. on Antennas and Propagat.*, Vol. 43, No. 12, 1474–1478, Dec. 1995.
10. Wang, H., Y. Ji, and T. H. Hubing, "Finite-element modeling of coaxial cable feeds and vias in power-bus structures," *IEEE Trans. Electromagn. Compat.*, Vol. 44, No. 4, 569–574, Nov. 2002.
11. Abd El-Raouf, H. E., V. V. S. Prakash, J. Yeo, and R. Mittra, "FDTD simulation of a microstrip phased array with a coaxial

feed," *IEE Proc., Microw. Antennas Propag.*, Vol. 151, No. 3, 193–198, Jun. 2004.

12. Hajiaboli, A. and M. Popovi'c, "FDTD subcell modeling of the inner conductor of the coaxial feed: Accuracy and convergence analysis," *IEEE Trans. on Magnetics*, Vol. 43, No. 4, 1361–1364 Apr. 2007.
13. Zhang, Y.-J. and J. Fan, "An intrinsic circuit model for multiple vias in an irregular plate pair through rigorous electromagnetic analysis," *IEEE Trans. on Microwave Theory and Tech.*, Vol. 58, No. 8, 2251–2265, Aug. 2010.
14. Zhang, Y.-J., G. Feng, and J. Fan, "A novel impedance definition of a parallel plate pair for an intrinsic via circuit model," *IEEE Trans. on Microwave Theory and Tech.*, Vol. 58, No. 12, 3780–3789, Dec. 2010.
15. Zhang, Y., J. Fan, G. Selli, M. Cocchini, and F. D. Paulis, "Analytical evaluation of via-plate capacitance for multilayer printed circuit boards and packages," *IEEE Trans. on Microwave Theory and Tech.*, Vol. 56, No. 9, 2118–2128, Sep. 2008.
16. Jin, J. M., *The Finite Element Method in Electromagnetics*, John Wiley & Sons, Inc., 1993.
17. Peterson, A. F., S. L. Ray, and R. Mittra, *Computational Methods for Electromagnetics*, Chapter 3, IEEE Press, New York, USA, 1997.
18. Lei, G.-T., R. W. Techentin, P. R. Hayes, D. J. Schwab, and B. K. Gilbert, "Wave model solution to the ground/power plane noise problem," *IEEE Trans. on Instrum. and Meas.*, Vol. 44, No. 2, 300–303, Apr. 1995.
19. Zheng, D. and K. A. Michalski, "Analysis of arbitrarily shaped coax- fed microstrip antennas with thick substrates," *Electronics Letters*, Vol. 26, No. 12, 794–795, 1990.